Microstructure evolution of accumulative roll bonding processed pure aluminum during cryorolling

Hailiang Yu,[a] Hui Wang, Cheng Lu, A. Kiet Tieu, Huijun Li,[b] Ajit Godbole, and Xiong Liu
School of Mechanical, Materials & Mechatronics Engineering, University of Wollongong, New South Wales 2500, Australia

Charlie Kong
Electron Microscope Unit, University of New South Wales, Sydney, New South Wales 2052, Australia

Xing Zhao
Key Laboratory of High Performance Complex Manufacturing, Central South University, Changsha 410083, Hunan, China; and School of Mechanical, Materials & Mechatronics Engineering, University of Wollongong, New South Wales 2500, Australia

(Received 27 August 2015; accepted 8 February 2016)

The microstructure evolution and mechanical properties of ultrafine-grained (UFG) Al sheets subjected to accumulative roll bonding (ARB) and subsequent cryorolling was studied. Cryorolling can suppress the dynamic softening of UFG Al sheets subjected to ARB at room temperature. After the third ARB pass, the grains are slightly refined as the number of ARB passes increases. However, the grains are significantly refined further during cryorolling. The grain size of 460 nm achieved after the third ARB pass is reduced to 290 nm after two cryorolling passes with total reduction ratio 80%. Sheets subjected to ARB + cryorolling show improved mechanical properties compared to only ARB-processed sheets due to a change in the fraction of high-angle boundaries and elongated grains. The deformation mechanism for ultrafine grains at room temperature is determined by grain boundary sliding or dislocation-based recovery, while it is governed by dislocation glide at cryogenic temperature.

I. INTRODUCTION

Globally, more than 20% of metal products are in the form of sheets, which are widely used in the automobile, aerospace, and other industries. Sheets made of ultrafine-grained/nano-grained (UFG/NG) materials have many desirable properties. A number of severe plastic deformation (SPD) techniques have been developed for manufacturing UFG materials: equal channel angular press (ECAP),[1–4] high pressure torsion (HPT),[5–7] accumulative roll bonding (ARB),[8–10] improved ARB (e.g., cross-ARB and four-layer ARB),[11–13] asymmetric rolling (AR),[14–17] cryorolling,[18–20] asymmetric cryorolling (ACR),[21–23] twist extrusion[24] and multiaxial incremental forging and shearing (MIFS).[25] Among these SPD techniques, ARB, AR, cryorolling, and ACR can be used to fabricate UFG metal sheets.

Aluminum alloys have been widely used to study the mechanism of grain refinement brought about by SPD, during which dynamic softening occurs with a higher equivalent strain when the strain exceeds a certain threshold value at room temperature. Ito and Horita[7] studied the microstructural evolution in pure Al processed by HPT. They found that the maximum Vickers microhardness of the samples reaches 45 Hv when the equivalent strain is 2.5, and gradually reduces with further increase in the equivalent strain. Montazeri-Pour et al.[25] studied the effect of MIFS on an AA1100 alloy sample at room temperature. They found that the ultimate tensile strength of the samples increases from 56 MPa to 189 MPa after four MIFS passes. However, with a further increase in the number of MIFS passes, the ultimate tensile strength decreases. Edalati and Horita[26] gave a detailed discussion of the "stacking fault energy" which affects the dislocation mobility and the dynamic softening that occurs more quickly to reach a steady state in Al-rich alloys.

With the development of SPD techniques, it was found that a combination of SPD with subsequent rolling can significantly improve the mechanical properties of UFG materials. Ranjbar Bahadori et al.[27] studied the relationship between the microstructure and the mechanical properties of commercial pure (CP) Cu processed using ECAP and subsequent cold rolling. Post-ECAP cold rolling not only reduced the grain size but also decreased the heterogeneity of grain distribution throughout the workpiece. Consequently, both the strength and the ductility of the workpiece improved significantly. Cold rolling of ECAP-processed specimens changed the microstructure from equiaxed grains to an elongated

Contributing Editor: George M. Pharr
Address all correspondence to these authors.
[a]e-mail: yuhailiang1980@tom.com, hailiang@uow.edu.au
[b]e-mail: huijun@uow.edu.au
DOI: 10.1557/jmr.2016.70

 © Materials Research Society 2016

https://doi.org/10.1557/jmr.2016.70 Published online by Cambridge University Press

structure with lamellar boundaries. Park et al.[28] subjected a commercial Al–Mg alloy sample to four passes of ECAP, followed by 70% rolling reduction in thickness. Post-ECAP rolling was found to enhance the high strain rate superplastic elongation significantly. Park et al.[28] also found that the deformation of the ECAP-processed sample was governed by viscous dislocation glide, while that of the sample subjected to (ECAP + cold rolling) was dominated by grain boundary sliding, which resulted in a relatively uniform deformation throughout the sample. Hajizadeh and Eghbali[29] investigated the microstructure and mechanical properties of CP Ti after processing by warm ECAP and cryorolling with a thickness reduction of 35%. After 10 passes of ECAP, an UFG structure with an average grain size of 213 nm was achieved with mainly equiaxed grains. Subsequent cryorolling led to further refinement and decreased the grain size to 114 nm with a lamellar structure and higher dislocation density. Renk et al.[30] found that the microstructure of HPT-processed samples subjected to subsequent rolling evolved into a new steady state which led to a larger grain size compared to that of only HPT-processed samples. Yu et al.[31,32] studied ARB-processed sheets during subsequent AR. Most of the elongated grains were further refined in the AR process. But some of the elongated grains were found to coarsen abnormally, resulting in an inhomogeneous microstructure. The inhomogeneous microstructure led to a bimodal structure with a higher strength and greater ductility.[33] Huang et al.[34] carried out a study of the mechanical properties of ARB-processed pure Al sheets under 10, 15, and 50% reduction in thickness by cold rolling at room temperature. Mechanical testing showed that subsequent cold rolling to low strains (10 and 15%) leads to softening and greater elongation compared to the as ARB-processed material. On the contrary, the cold rolling to achieve a large strain of 50% results in significant strengthening. Dislocations are introduced during the cold rolling and the dislocation density increases with the rolling reduction. However, there is a change in the dislocation configurations when the strain is increased from 15% to 50%. At a low strain, the interior dislocations are principally present as loose dislocations which are supposed to be free to move when a stress is applied. At high strain, the dislocations form tangles and networks. This change in the characteristics of dislocation structure is considered to be the cause for the transition from softening to hardening. However, there are no reports to date related to the evolution in mechanical properties and microstructure of ARB-processed sheets during subsequent cryorolling.

Deformation at cryogenic temperature has emerged as a potential method to develop UFG materials with a high dislocation density with improved mechanical properties. Cryorolling at liquid nitrogen temperature suppresses the dynamic recovery during deformation, thereby enhancing grain refinement. Cryorolling paves the way for industrial applications of cold surface hardening.[35] Marnett et al.[18] showed that the cryorolled material acquires a tensile strength which is 30% higher compared to room temperature rolled material. Panigrahi and Javaganthan[19] studied the effect of rolling temperature on the mechanical properties and microstructural characteristics of Al 6063 sheets when severely rolled to achieve up to 92% thickness reduction, both at cryogenic temperature and room temperature. An improved strength (257 MPa) of cryorolled 6063 Al alloy was obtained compared to the room temperature rolled alloy (232 MPa). In this paper, we present a novel investigation on the mechanical properties and microstructure evolution of ARB-processed CP Al during subsequent cryorolling. We found that the grains of ARB-processed CP Al further refine with subsequent cryorolling, however, which cannot refine with more ARB passes. Finally, we discussed with microstructure evolution mechanism of UFG Al materials during deformation at room and cryogenic temperatures, respectively.

II. EXPERIMENTAL

The evolution in the microstructure and mechanical properties of 1 mm thick ARB-processed AA1060 sheets during subsequent cryorolling were studied. The alloy composition (mass%) was: Al 99.6, Si 0.25, Cu 0.05, Mn 0.03, Mg 0.03, and others. Before rolling, the Al sheets were annealed at 873 K for two hours, and the resulting mean grain size was 30 μm. Two rolling schedules were designed: (i) five ARB passes; (ii) three ARB passes plus two subsequent cryorolling passes. The ARB process was carried out at room temperature, and the cryorolling was processed at a cryogenic temperature of 77 K. Figure 1 shows an illustration of UFG Al sheet fabrication using ARB and subsequent cryorolling. Before ARB, the sheets were cut into two halves, surface treated, and stacked. The stacks were dry friction-rolled to achieve 50% thickness reduction per pass. After each ARB pass, these steps were repeated. For cryorolling, the ARB-processed sheets were then immersed in liquid nitrogen for at least 10 min before rolling. Then the sheets were quickly rolled, first to 0.5 mm after the first cryorolling pass, and then to 0.2 mm thickness after the second cryorolling pass.

After one month subsequent to cryorolling, the microstructure tests were carried out for both ARB-processed and ARB + cryorolled samples on the same day. The microstructure evolution of samples after annealing, the third ARB pass, the fifth ARB pass, the first cryorolling pass, and the second cryorolling pass was tested using a Philips CM200 field emission gun transmission electron microscope (FEI Company, Amsterdam, The Netherlands) equipped with a Bruker energy dispersive x-ray spectroscopy system (Bruker Corporation, Billerica, Massachusetts) operating at an accelerating voltage of 200 kV. The transmission electron microscope (TEM) samples were prepared by focused ion beam (FIB)

https://doi.org/10.1557/jmr.2016.70 Published online by Cambridge University Press

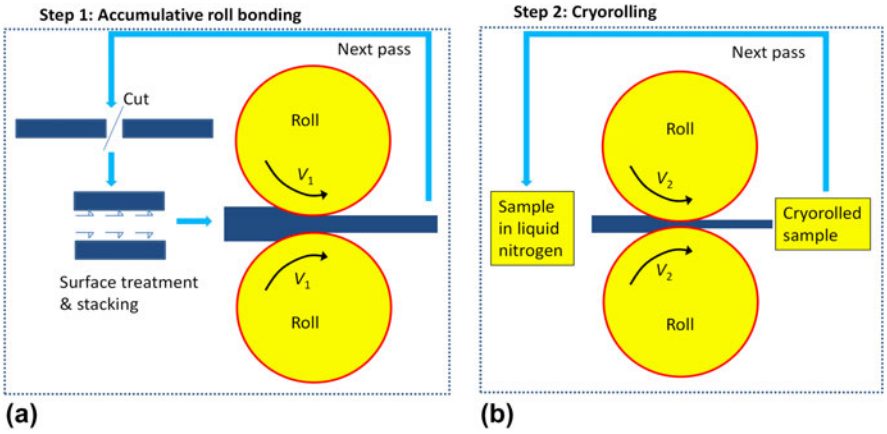


FIG. 1. Illustration of fabrication of UFG Al sheets by combined ARB (a) and cryorolling (b) techniques.

technique on an FEI xT Nova Nanolab 200 dual-beam workstation (FEI Company, Hillsboro, Oregon). The FIB slices were made in the normal direction (ND) to the rolling direction (RD). TEM images were observed in transverse direction, in the plane of RD × ND. The residual dislocation density was measured based on a survey of the visible dislocation lines in bright field electron micrographs under two random diffraction conditions. Due to the nature of the deformed UFG microstructure of the Al alloys, it is not applicable to make the measurement based on two-beam conditions, which is the standard method to verify the invisibility of dislocations in TEM for materials with large grain or single crystals. However, the measurements on a series of test samples did show a trend which correlates with the mechanical properties of UFG materials. This provides a means to interpret a mechanism of material strengthening with cryorolling. The mechanical properties of the samples after ARB and cryorolling processing were tested. Tensile tests with a strain rate of 1.0×10^{-3} s^{-1} were carried out on the foil samples using an Instron machine (Cambridge, Massachusetts). The morphology of the fractured surface of samples was studied with a Hitachi N3400 scanning electron microscope (Hitachi, Tokyo, Japan). The fracture surface was observed from the tensile direction. The finite element method (FEM) was used to calculate the temperature increase of strip during cryorolling using LS-DYNA (Livermore Software Technology Corp., Canonsburg, Pennsylvania). In the models, there are 127,692 nodes and 102,900 elements. The heat capacity of the sheet material was set as 91 J/(gK), and the thermal conductivity as 300 W/(mK), the initial temperature of sheet as 77 K, and the friction coefficient between the sheet and roll was set as 0.3. During rolling, the fraction of mechanical work converted into heat was set as 0.9.[36]

III. RESULTS

Figure 2 shows TEM images of the samples during the process. Figure 2(a) shows the coarse grains before ARB. After the third ARB pass, the mean grain size was reduced to 460 nm, as shown in Fig. 2(b). After 5 ARB passes, the microstructure contains nearly equiaxed grains with a mean grain size of 420 nm, as shown in Fig. 2(c). Saito et al.[9] and Pirgazi et al.[10] found that the mean grain size of ARB-processed AA1050 sheets can be refined to between 670 and 500 nm when the rolling temperature is 473 K. In the present study, the sheets were not heated before ARB processing. Thus, the mean grain size of the samples after ARB is slightly less than the values reported by Saito et al.[9] and Pirgazi et al.[10] However, it should be noted that the purity of AA1060 is higher than AA1050. Figure 2(d) shows the microstructure of the ARB-processed samples after the first cryorolling pass. It can be seen that the grains are significantly refined. After the second cryorolling pass, the grains are transformed into an elongated structure of 290 nm, as shown in Fig. 2(e), much smaller than that in Fig. 2(c). During SPD, the grains of Al alloys are refined to a certain minimum size. The grain size cannot be refined any further due to dynamic recovery.[37,38] As shown in Figs. 2(b) and 2(c), the grain size changes slightly when the equivalent strain increases from 2.4 to 4.0. However, we also found that the grains in ARB-processed samples can be significantly refined with lamellar structure during cryorolling, as shown in Figs. 2(d) and 2(e). This implies that the dynamic recovery in the Al sheets is effectively suppressed during cryogenic deformation. The grain size distributions of samples after processing are shown in Fig. 3. During ARB processing, most of grains range from 400 nm to 500 nm in size, as shown in Figs. 3(a) and 3(b). When using cryorolling, the grains are mostly in the range of 200–300 nm, as shown in Figs. 3(c) and 3(d).

Figure 4 shows the mean grain size of CP Al (AA1050 & AA1060) subjected to several SPD techniques. Using the HPT technique,[7] the grain size at the sample edge is about 100–200 nm, while at the sample center it is 600 nm for AA1050, when the equivalent strain is in the range 4.2–5.8. When subjected to ACR, the mean grain

https://doi.org/10.1557/jmr.2016.70 Published online by Cambridge University Press

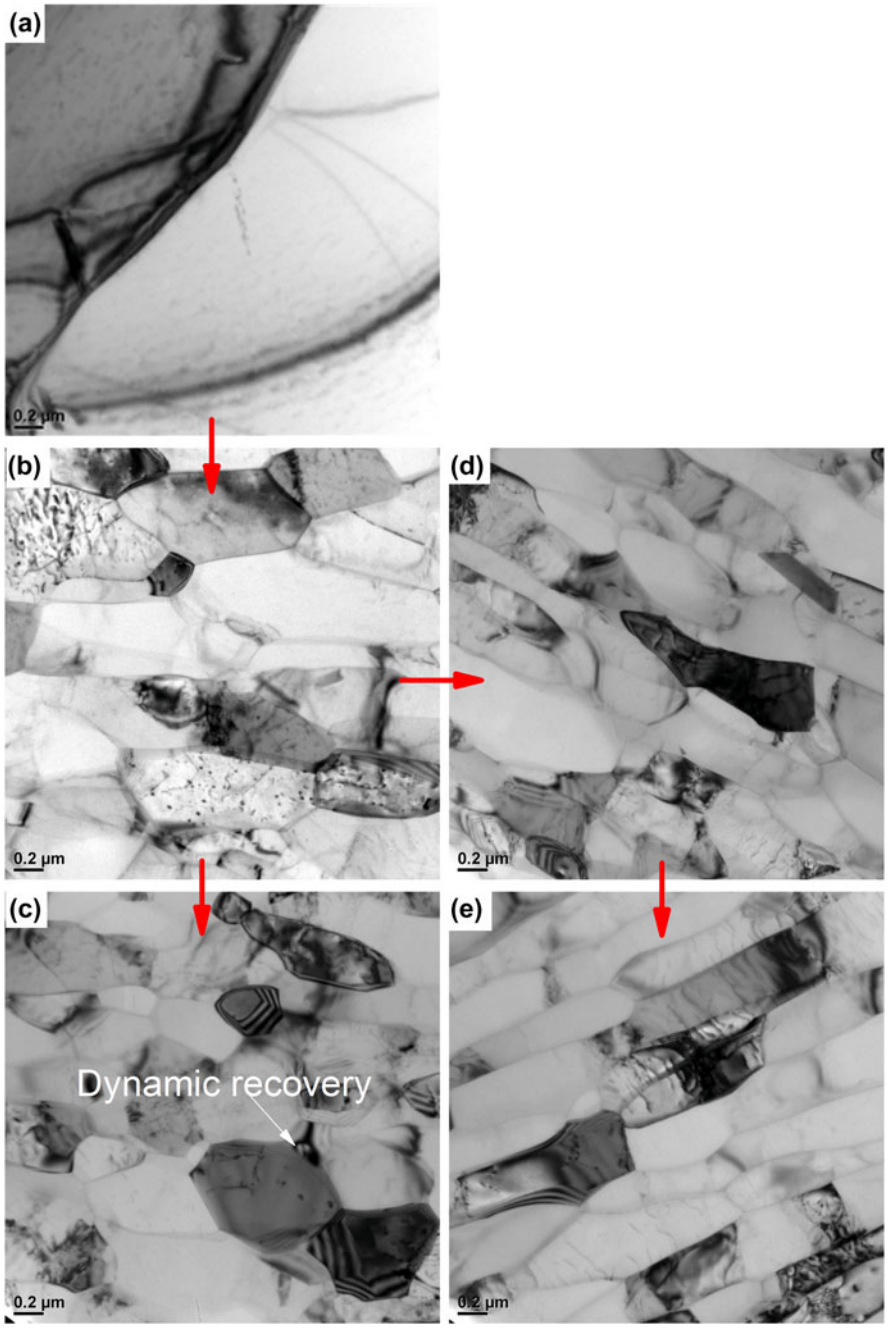


FIG. 2. TEM images of samples. (a) Annealed; (b) after the 3rd ARB pass; (c) after the 5th ARB pass; (d) after the 3rd ARB pass plus the 1st cryorolling pass; (e) after the 3rd ARB pass plus the 2nd cryorolling pass.

size of AA1050 is in the range 211–360 nm when the thickness of sheets was rolled to 0.17 mm from 1.5 mm (equivalent strain ~ 2.5).[23] Using the ARB technique, a mean grain size of 670 and 500 nm was achieved in AA1050 sheets after six and ten passes (equivalent strain 4.8 and 8), respectively.[9,10] With the ECAP technique, the average grain size of the AA1050 sample reaches 600 nm, with the equivalent strain reaching 11.2.[4] Lee and Lee[17] observed fine 1400 nm grains in AA1050 using the AR technique when the thickness of sheets was reduced from 2.0 mm to 0.75 mm (equivalent strain ~ 1.2). In these studies, the AA1050 samples were used for HPT,[7] ACR,[23] ARB,[9,10] ECAP,[4] AR[17] techniques, which has lower impurities compared to AA1060 used in the present study. Generally, the smaller grain size can be obtained for the CP Al alloy with lower impurities, for the same processing parameters. Using ECAP, a mean grain size of 660 nm can be obtained for AA1070 (Ref. 3)

https://doi.org/10.1557/jmr.2016.70 Published online by Cambridge University Press

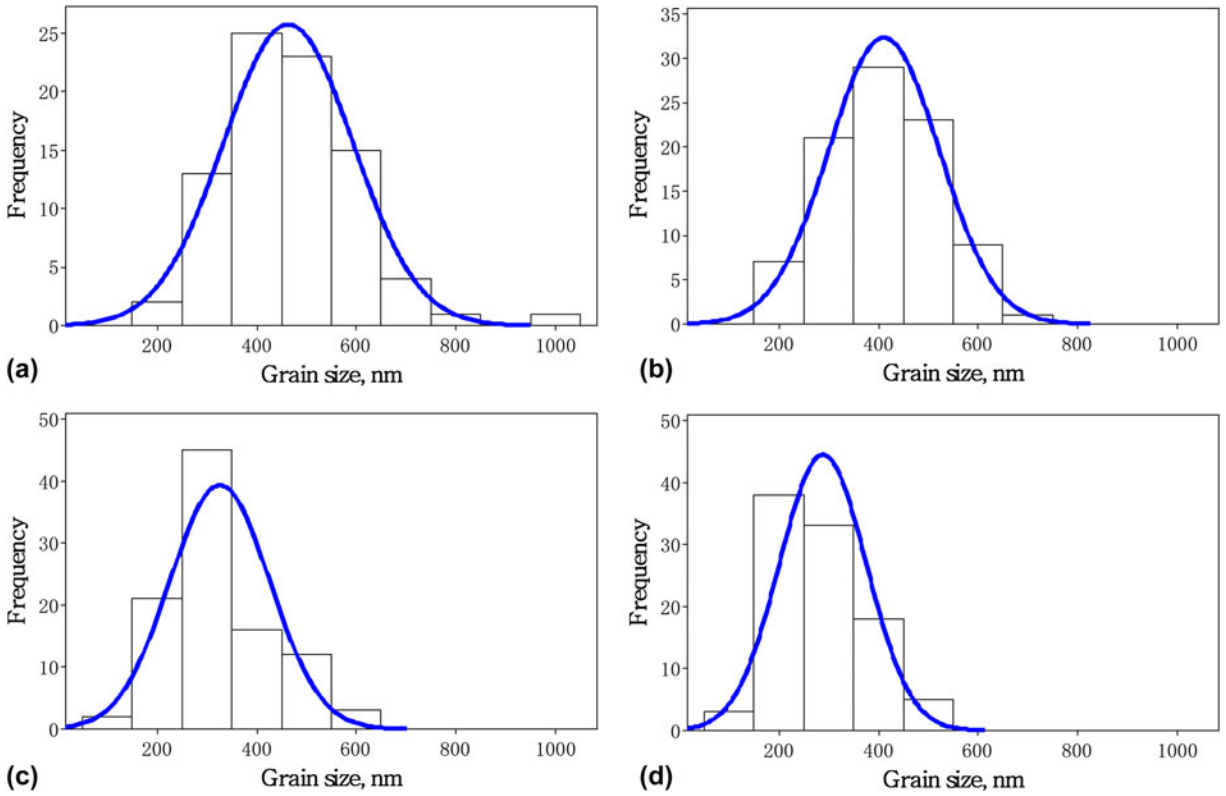


FIG. 3. Grain size distribution of sheets. (a) After the 3rd ARB pass; (b) after the 5th ARB pass; (c) after the 3rd ARB pass plus the 1st cryorolling pass; (d) after the 3rd ARB pass plus the 2nd cryorolling pass.

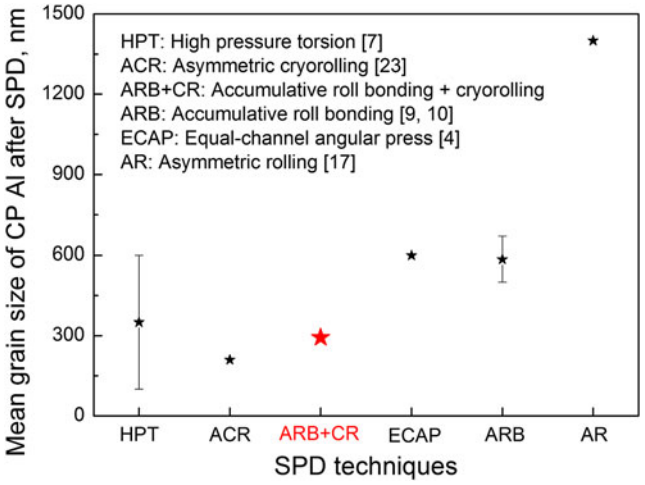


FIG. 4. Mean grains of CP Al after different SPD processes.

while a mean grain size of 600 nm for AA1050 (Ref. 4) subjected to a similar strain. In addition, the grain size gradually reduces with an increase in equivalent strain if there is no dynamic softening behavior in the deformation processes. The equivalent strain in the current study is 4.0 for ARB and 4.2 for ARB + cryorolling, which is less than the equivalent strain in the studies involving HPT,[7] ARB,[9,10] and ECAP.[4] Thus, it is seen that we can achieve much finer grains of Al alloys when they are subjected to the combination of ARB and cryorolling techniques.

Figure 5 shows the engineering stress versus engineering strain curves of the samples after being subjected to different processing conditions. Annealed samples have high ductility but lower strength. After the third ARB pass, the yield strength increases from 90 MPa to 184 MPa as the elongation is reduced from 55% to 20%. After the fifth ARB pass, the yield strength increases slightly to 186 MPa. When using (ARB + CR), the yield strength increases to 198 MPa after the first cryorolling pass, and to 206 MPa after the second cryorolling pass. For similar equivalent strain during deformation after the second cryorolling pass and the fifth ARB pass, the yield strength increases by more than 10%. Compared to the samples after the fifth ARB pass, both the strength and ductility of sheets are improved after the first cryorolling pass.

Figure 6 shows the fracture surface of the samples after the tensile test. After ARB, the samples generally show a lower ductility, as shown in Figs. 6(a) and 6(b), in which the fracture surface is smooth, with shallow dimples. However, when subjected to cryorolling, more dimples are seen at the fracture surface, as shown in Fig. 6(c), which implies an improved ductility during cryorolling. After the second cryorolling pass, the sheets show severe necking although the engineering failure

https://doi.org/10.1557/jmr.2016.70 Published online by Cambridge University Press

strain during tensile test is 0.12. For UFG foils, it has been suggested that the area reduction ratio is a good measure of the ductility,[39] as shown in Eq. (1):

$$\varepsilon_{\text{axial}} = \ln(A_{\text{initial}}/A_{\text{final}}) = \ln\left(\frac{1}{1-q}\right) \quad , \qquad (1)$$

where A_{initial} is the cross-section area before the tensile test, q is the fractional change in cross-section area $[(A_{\text{initial}} - A_{\text{final}})/A_{\text{initial}}]$. The true failure strain after the second cryorolling pass reaches 1.1 which is larger than others, as shown in Fig. 6(d). In this study, the samples show a lower failure strain during the tensile test after the second cryorolling pass, possibly resulting from size effects.[40,41] Compared to the ARB-processed samples, the sheets were reduced to 0.2 mm from 1.0 mm after the second cryorolling pass. Suh et al.[41] found that the failure strain of sheets with thickness 0.4 mm was cut half compared to that of sheets with thickness 1.58 mm although they had the same microstructure. Generally, the ductility of UFG metals can be enhanced by deformation at cryogenic temperature.[29,42–44] Hajizadeh and Eghbali[29] found that post-ECAP cryorolling could improve both the ductility and strength of CP Ti. The yield stress, tensile stress, and failure strain are 750 MPa, 892 MPa, and 20.5% for 10 pass ECAP-processed samples, which increases to 802 MPa, 995 MPa, and 23% for ECAP + cryorolled samples. Zhao et al.[43] believed that the high ductility after cryogenic processing could be attributed primarily to the change in the fraction of high-angle boundaries and pre-existing deformation twins. In the present study, it is shown that changes in the fraction of high-angle boundaries[43] and the elongated structure[45] [as shown in Figs. 2(d) and 2(e)] contribute to the improvement in strength without reduction of the materials ductility.

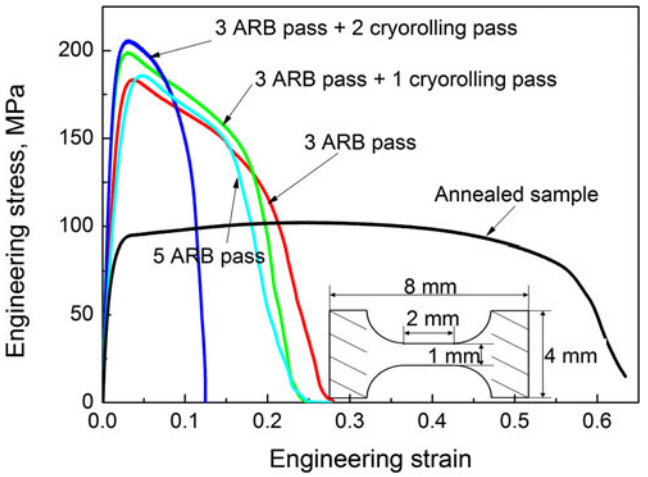


FIG. 5. Engineering stress versus engineering strain of Al sheets during tensile test.

IV. DISCUSSION

In the present study, it was found that the grains of the ARB + cryorolled sheets were further refined by more than 30% (after the second cryorolling pass) compared to only ARB-processed sheets (after the fifth ARB pass), although the strains induced in the sheets in the two cases were similar (equivalent strain 4.2 and 4.0 for ARB + cryorolled and ARB-only-processed sheets respectively). It is obvious that the deformation mechanism of UFG Al

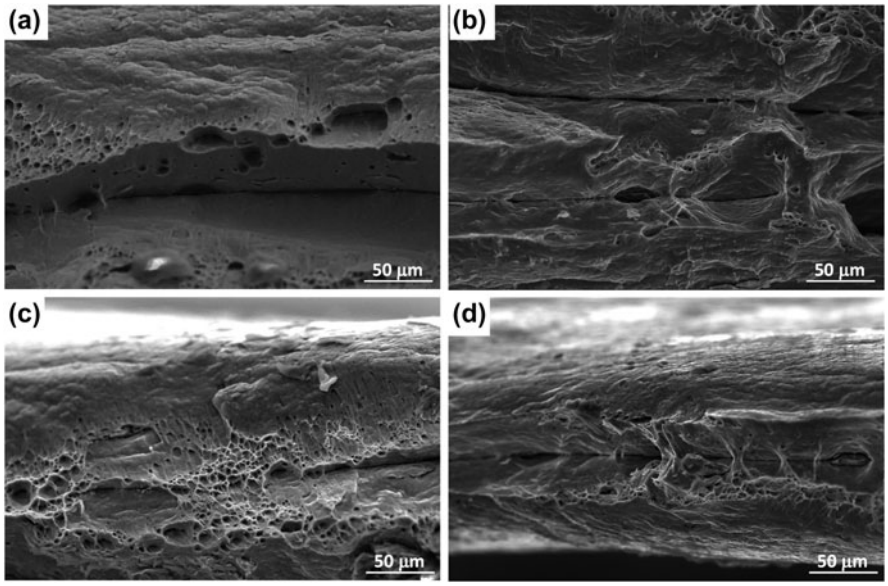


FIG. 6. Fracture surface of samples for (a) after the 3rd ARB pass; (b) after the 5th ARB pass; (c) after the 3rd ARB pass plus the 1st cryorolling pass; (d) after the 3rd ARB pass plus the 2nd cryorolling pass.

https://doi.org/10.1557/jmr.2016.70 Published online by Cambridge University Press

sheets subjected to cryorolling is different from sheets subjected to further ARB processing. This could be due to a difference in the deformation temperature.

Generally, with decreasing grain size of UFG/NG bulk metals, the deformation mechanism will change from dislocation slip to a grain-boundary-based deformation process at room temperature.[46] For UFG metals, many deformation mechanisms have been proposed, such as grain boundary sliding, grain rotation, diffusional creep, twinning, full and partial dislocation emission from grain boundaries and related stacking fault formation[47] as well as normal dislocation slip.[48,49] One side, at room temperature, plasticity might be governed mainly by processes at the grain boundaries, where the first isolated sliding events are initiated along the "softest" grain boundaries and then stop at some obstacle such as triple points or grain ledges. Then a higher stress is necessary to overcome such obstacles or to activate sliding along the less "soft" grain boundaries.[50] In UFG materials, grain boundary sliding during deformation has been observed in experiments[51] and molecular dynamic (MD) simulation.[51–54] Generally, for metals, grain boundary sliding may be the primary mechanism during deformation when the temperature rises or the grain size reduces.[51] Under room temperature uniaxial compressions of 900 nm-diameter Al bicrystals each containing a high-angle grain boundary with a plane normal inclined with respect to the loading direction, Aitken et al.[50] observed frictional grain boundary sliding where the top crystallite is sheared off as a single unit along the grain boundary. On the other hand, some researchers believed that dislocation-based deformation mechanism still plays a key role for UFG materials during SPD,[49] while the recovery results in no further refinement of grains. When the induced strain is larger than a critical strain, the dynamic recovery occurs at room temperature for UFG materials, as shown in Fig. 2(c). Simultaneous activation of planar slip along with grain boundary mediated deformation during large strain deformation of nanocrystalline Ni was reported by Gurao and Suwas.[48] They emphasized that the major contribution to deformation in nanocrystalline Ni with a grain size of ~20 nm occurs through normal dislocation slip. The activation of slip contributes to dislocation annihilation that leads to mechanical recovery. The critical strain for dynamic recovery increases with strain rate or the Zener–Hollomon parameter,[55] which is defined as:

$$Z = \dot{\varepsilon} \exp\left(\frac{Q}{RT}\right) \quad , \tag{2}$$

where Q is the activation energy. It is obvious that the critical strain will increase with decreasing deformation temperature (T). Thus, both grain boundary sliding and dynamic recovery behavior can result in a slight change in grain size during deformation at room temperature, although the equivalent strain reaches 1.6 for samples subjected to further ARB passes.

At low temperature and for large grain size, deformation tends to occur preferentially by dislocation glide rather than by grain boundary sliding.[51] The cryogenic temperature decreases the dislocation mobility and hence reduces the rate of dynamic recovery. This then allows the density of the accumulated dislocations to reach higher levels than at room temperature.[55] As shown in Figs. 2(d) and 2(e), there is no dynamic recovery in the grains. Equation (3) shows the dislocation density (ρ) of UFG materials as a function of shear strain (γ)[49]:

$$\frac{d\rho}{d\gamma} = k_1\sqrt{\rho} - k_2\rho \quad , \tag{3}$$

where k_1 is a constant accounting for interaction of gliding dislocations with the forest ones. k_2 is related to the dynamic recovery leading to a loss of dislocation density due to annihilation by processes, which is a function of the absolute temperature T and average dislocation velocity (V) as follows:

$$k_2 = \frac{2+2\alpha}{1+2\alpha}\frac{bv_0}{\langle V\rangle}\exp\left(-\frac{\Delta G}{k_B T}\right) \quad , \tag{4}$$

where v_0 is the pre-exponential factor of the order of the Debye frequency, ΔG is the activation energy for the governing mechanism of annihilation, which can be identified with activation energy for self-diffusion, and k_B is the Boltzmann constant. Without loss of generality, k_2 can be related to any second-order kinetics of dislocation annihilation, including the dislocation annihilation in the grain/cell boundaries. From Eqs. (3) and (4), it is obvious that the dislocation annihilation will reduce as the temperature decreases. Generation and evolution of dislocation rather than recrystallization has been generally attributed to the grain refinement at cryogenic temperature.[56] In the present study, it was found that the dislocation density after annealing was 1.0×10^{12} m^{-2}, and it increased to 5.7×10^{13} m^{-2} after the third ARB pass. With further deformation at room temperature, the dislocation density increased slightly, to about 8.0×10^{13} m^{-2} after the fifth ARB pass. However, the deformation at cryogenic temperatures can effectively suppress dislocation annihilation. The dislocation density after the first cryorolling pass was 1.0×10^{14} m^{-2}, which increased to 1.1×10^{14} m^{-2} after the second cryorolling pass.

In addition, both grain boundary sliding and grain boundary dislocation nucleation are thermally activated processes. A significant increase in the applied stress is necessary to trigger these processes as the temperature decreases. Cheng et al.[54] carried out a MD simulation of

https://doi.org/10.1557/jmr.2016.70 Published online by Cambridge University Press

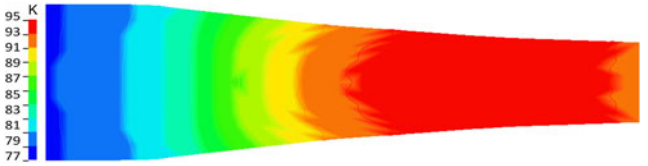


FIG. 7. Thermal field of sheets in the deformation zone during cryorolling. The reduction ratio is set as 50%, and the initial temperature of sheet is 77 K.

grain boundary sliding at different deformation temperatures. At a lower deformation temperature, grain boundary sliding becomes increasingly difficult. Grain boundary sliding will become completely "frozen" when the deformation temperature is less than a certain value. On the other hand, the rate of dislocation emission from grain boundaries increases due to the higher applied strain. At very low temperatures, pure sliding is not observed, but dislocation nucleation and extension is observed on grain boundaries. Figure 7 shows the FEM-simulated temperature field in the sheet during cryorolling with a reduction ratio of 50%. Due to the plastic deformation work, the temperature of the sheets will increase in the deformation zone. However, the maximum temperature in the sheets is still lower than 100 K during cryorolling. At temperatures below 100 K,[53] the stress–time curves display larger stress reduction over longer periods. The atoms at temperatures below 100 K are difficult to move, so that the grain boundaries can accumulate and release more elastic energy in one period.[53] Thus, cryogenic deformation can make the grain size much finer. Darling et al.[57] reported that the cryogenic surface mechanical attrition treatment process resulted in a 60% reduction in the grain size in polycrystalline microstructure compared to that at room temperature.

V. CONCLUSIONS

(1) Cryogenic deformation can significantly suppress the dynamic recovery caused by SPD. Cryorolling of ARB-processed Al sheets can significantly refine the grains. After the third ARB pass, the grains can be refined to 460 nm, and then to 290 nm when subjected to cryorolling, as the sheet thickness reduces from 1.0 mm to 0.2 mm. In contrast, only a slight further reduction to 420 nm grain size is possible with more ARB passes.

(2) Compared to the samples after the fifth ARB pass, both the strength and ductility of sheets are improved after the first cryorolling pass, due to the change in the fraction of high-angle boundaries and elongated structure.

(3) The deformation mechanism of UFG metals at cryogenic temperature is different from that at room temperature. At cryogenic temperature, the deformation is dominated by dislocation glide, while it is mainly grain boundary sliding or dislocation-based recovery at room temperature.

ACKNOWLEDGMENTS

This study was funded by URC small grant at the University of Wollongong, and the Open Research Fund of Key Laboratory of High Performance Complex Manufacturing, Central South University.

REFERENCES

1. R.Z. Valiev and T.G. Langdon: Principles of equal-channel angular pressing as a processing tool for grain refinement. *Prog. Mater. Sci.* **51**, 881 (2006).
2. Y. Iwahashi, Z. Horita, M. Nemoto, and T.G. Langdon: The process of grain refinement in equal-channel angular pressing. *Acta Mater.* **46**, 3317 (1998).
3. M. Hockauf and L.W. Meyer: Work-hardening stages of AA1070 and AA6060 after severe plastic deformation. *J. Mater. Sci.* **45**, 4778 (2010).
4. E.A. EI-Danaf: Mechanical properties and microstructure evolution of 1050 aluminum severely deformed by ECAP to 16 passes. *Mater. Sci. Eng., A* **487**, 189 (2008).
5. A.P. Zhilyaev and T.G. Langdon: Using high-pressure torsion for metal processing: Fundamentals and applications. *Prog. Mater. Sci.* **53**, 893 (2008).
6. Y. Estrin and A. Vinogradov: Extreme grain refinement by severe plastic deformation: A wealth of challenging science. *Acta Mater.* **61**, 782 (2013).
7. Y. Ito and Z. Horita: Microstructural evolution in pure aluminum processed by high-pressure torsion. *Mater. Sci. Eng., A* **503**, 32 (2009).
8. N. Tsuji, Y. Saito, S.H. Lee, and Y. Minamino: ARB (accumulative roll-bonding) and other new techniques to produce bulk ultrafine grained materials. *Adv. Eng. Mater.* **5**, 338 (2003).
9. Y. Saito, N. Tsuji, H. Utsunomiya, T. Sakai, and R.G. Hong: Ultra-fine grained bulk aluminum produced by accumulative roll-bonding (ARB) process. *Scr. Mater.* **39**, 1221 (1998).
10. H. Pirgazi, A. Akbarzadeh, R. Petrov, and L. Kestens: Microstructure evolution and mechanical properties of AA1100 aluminum sheet processed by accumulative roll bonding. *Mater. Sci. Eng., A* **497**, 132 (2008).
11. H. Azzeddine, K. Tirsatine, T. Baudin, A. Helbert, F. Brisset, and D. Bradai: Texture evolution of an Fe–Ni alloy sheet produced by cross accumulative roll bonding. *Mater. Charact.* **97**, 140 (2014).
12. R. Jamaati, M.R. Toroghinejad, S. Amirkhanlou, and H. Edris: On the achievement of nanostructured interstitial free steel by four-layer accumulative roll bonding process at room temperature. *Metall. Mater. Trans. A* **46**, 4013 (2015).
13. H.L. Yu, C. Lu, K. Tieu, and C. Kong: Fabrication of nanostructured aluminum sheets using four-layer accumulative roll bonding. *Mater. Manuf. Process.* **29**, 448 (2014).
14. Q.B. Yu, X.H. Liu, and D.L. Tang: Extreme extensibility of copper foil under compound forming conditions. *Sci. Rep.* **3**, 3556 (2013).
15. D.L. Tang, X.H. Liu, M. Song, and H.L. Yu: Experimental and theoretical study on minimum achievable foil thickness during asymmetric rolling. *PLoS One* **9**, e106637 (2014).
16. F.Q. Zou, J.H. Jiang, A.D. Shan, J.M. Fang, and X.Y. Zhang: Shear deformation and grain refinement in pure Al by asymmetric rolling. *Trans. Nonferrous Met. Soc. China* **18**, 774 (2008).
17. J.K. Lee and D.N. Lee: Texture control and grain refinement of AA1050 Al alloy sheets by asymmetric rolling. *Int. J. Mech. Sci.* **50**, 869 (2008).
18. J. Marnett, M. Weiss, and P.D. Hodgson: Roll-formablility of cryo-rolled ultrafine aluminium sheet. *Mater. Des.* **63**, 471 (2014).

https://doi.org/10.1557/jmr.2016.70 Published online by Cambridge University Press

19. S.K. Panigrahi and R. Jayaganthan: A study on the combined treatment of cryorolling, short-annealing, and aging for the development of ultrafine-grained Al 6063 alloy with enhanced strength and ductility. *Metall. Mater. Trans. A* **41**, 2675 (2010).
20. P. Trivedi, S. Goel, S. Das, R. Jayaganthan, D. Lahiri, and P. Roy: Biocompatibility of ultrafine grained zircaloy-2 produced by cryorolling for medical applications. *Mater. Sci. Eng., C* **46**, 309 (2015).
21. H.L. Yu, K. Tieu, C. Lu, X. Liu, M. Liu, A. Godbole, C. Kong, and Q. Qin: A new insight into ductile fracture of ultrafine-grained Al–Mg alloys. *Sci. Rep.* **5**, 9568 (2015).
22. H.L. Yu, K. Tieu, C. Lu, X.H. Liu, A. Godbole, and C. Kong: Mechanical properties of Al–Mg–Si alloy sheets produced using asymmetric cryorolling and ageing treatment. *Mater. Sci. Eng., A* **568**, 212 (2013).
23. H.L. Yu, C. Lu, K. Tieu, X. Liu, Y. Sun, Q. Yu, and C. Kong: Asymmetric cryorolling for fabrication of nanostructural aluminum sheets. *Sci. Rep.* **2**, 772 (2012).
24. D. Orlov, Y. Beygeizimer, S. Synkov, V. Varyukhin, N. Tsuji, and Z. Horita: Microstructure evolution in pure Al processed with twist extrusion. *Mater. Trans.* **50**, 96 (2009).
25. M. Montazeri-Pour, M.H. Parsa, H.R. Jafarian, and S. Taieban: Microstructural and mechanical properties of AA1100 aluminum processed by multi-axial incremental forging and shearing. *Mater. Sci. Eng., A* **639**, 705 (2015).
26. K. Edalati and Z. Horita: Significance of homologous temperature in softening behavior and grain size of pure metals processed by high-pressure torsion. *Mater. Sci. Eng., A* **528**, 7514 (2011).
27. S. Ranjbar Bahadori, K. Dehghani, and F. Bakhshandeh: Microstructural homogenization of ECAPed copper through post-rolling. *Mater. Sci. Eng., A* **588**, 260 (2013).
28. K.T. Park, H.J. Lee, C.S. Lee, W.J. Nam, and D.H. Shin: Enhancement of high strain rate superplastic elongation of a modified 5154 Al by subsequent rolling after equal channel angular pressing. *Scr. Mater.* **51**, 479 (2004).
29. K. Hajizadeh and B. Eghbali: Effect of two-step severe plastic deformation on the microstructure and mechanical properties of commercial purity titanium. *Metal Mater. Int.* **20**, 343 (2014).
30. O. Renk, A. Hohenwarter, S. Wurster, and R. Pippan: Direct evidence for grain boundary motion as the dominant restoration mechanism in the steady-state regime of extremely cold-rolled copper. *Acta Mater.* **77**, 401 (2014).
31. H.L. Yu, C. Lu, K. Tieu, A. Godbole, Y. Sun, M. Liu, L.H. Su, D.L. Tang, and C. Kong: Fabrication of ultrathin nanostructured bimetal foils by accumulative roll bonding and asymmetric rolling. *Sci. Rep.* **3**, 2373 (2013).
32. H.L. Yu, K. Tieu, C. Lu, and A. Godbole: An investigation of interface bonding of bimetallic foils by combined accumulative roll bonding and asymmetric rolling techniques. *Metall. Mater. Trans. A* **45**, 4038 (2014).
33. H.L. Yu, K. Tieu, S. Hadi, C. Lu, A. Godbole, and C. Kong: High strength and ductility of ultrathin laminate foils using accumulative roll bonding and asymmetric rolling. *Metall. Mater. Trans. A* **46**, 869 (2015).
34. X. Huang, N. Kamikawa, and N. Hansen: Property optimization of nanostructured ARB-processed Al by post-process deformation. *J. Mater. Sci.* **43**, 7397 (2008).
35. D. Meryer: Cryogenic deep rolling—An energy based approach for enhanced cold surface hardening. *CIRP Annal. Manuf. Technol.* **61**, 543 (2012).
36. H.L. Yu and X.H. Liu: Thermal-mechanical finite element analysis of evolution of surface cracks during slab rolling. *Mater. Manuf. Processes* **24**, 570 (2009).
37. Z.C. Sun, L.S. Zhang, and H. Yang: Softening mechanism and microstructure evolution of as-extruded 7075 aluminum alloy during hot deformation. *Mater. Charact.* **90**, 71 (2014).
38. C. Shi, J.L. Lai, and X.G. Chen: Microstructural evolution and dynamic softening mechanisms of Al–Zn–Mg–Cu alloy during hot compressive deformation. *Materials* **7**, 244 (2014).
39. J.A. Sharon, H.A. Padilla, and B.L. Boyce: Interpreting the ductility of nanocrystalline metals. *J. Mater. Res.* **28**, 1539 (2013).
40. H.L. Yu, K. Tieu, C. Lu, Y.S. Lou, X.Y. Liu, A. Godbole, and C. Kong: Tensile fracture of ultrafine grained aluminum 6061 sheets by asymmetric cryorolling for microforming. *Int. J. Damage Mech.* **23**, 1077 (2014).
41. C.H. Suh, Y.C. Jung, and Y.S. Kim: Effects of thickness and surface roughness on mechanical properties of aluminum sheets. *J. Mech. Sci. Technol.* **24**, 2091 (2010).
42. Y. Wang, M. Chen, F. Zhou, and E. Ma: High tensile ductility in a nanostructured metal. *Nature* **419**, 912 (2002).
43. Y.H. Zhao, J.F. Bingert, X.Z. Liao, B.Z. Cui, K. Han, A.V. Sergueeva, A.K. Mukherjee, R.Z. Valiev, T.G. Langdon, and Y.T. Zhu: Simultaneously increasing the ductility and strength of ultra-fine-grained pure copper. *Adv. Mater.* **18**, 2949 (2006).
44. I.A. Ovid'ko and T.G. Langdon: Enhanced ductility of nanocrystalline and ultrafine-grained metals. *Rev. Adv. Mater. Sci.* **30**, 103 (2012).
45. X.C. Liu, H.W. Zhang, and K. Lu: Strain-induced ultrahard and ultrastable nanolaminated structure in nickel. *Science* **342**, 337 (2013).
46. V. Yamakov, D. Wolf, S.R. Phillpot, A.K. Mukherjee, and H. Gleiter: Deformation-mechansim map for nanocrystalline metals by molecular-dynamics simulation. *Nat. Mater.* **3**, 43 (2004).
47. Y. Ivanisenko, E.D. Tabachnikova, I.A. Psaruk, S.N. Smirnov, A. Kilmametov, A. Kobler, C. Kübel, L. Kurmanaeva, K. Csach, Y. Mishkuf, T. Scherer, Y.A. Semerenko, and H. Hahn: Variation of the deformation mechanisms in a nanocrystalline Pd–10 at.% Au alloy at room and cryogenic temperature. *Int. J. Plast.* **60**, 40 (2014).
48. N.P. Gurao and S. Suwas: Deformation mechanisms during large strain deformation of nanocrystalline nickel. *Appl. Phys. Lett.* **94**, 191902 (2009).
49. A. Vinogradov: Mechanical properties of ultrafine-grained metals: New challenges and perspectives. *Adv. Eng. Mater.* **17**, 1710 (2015).
50. Z.A. Aitken, D. Jang, C.R. Weinberger, and J.R. Greer: Grain boundary sliding in aluminum nano-bi-crystals deformed at room temperature. *Small* **10**, 100 (2014).
51. H. Ghaffarian, A.K. Taheri, K. Kang, and S. Ryu: Molecular dynamics simulation study of the effect of temperature and grain size on the deformation behavior of polycrystalline cementite. *Scr. Mater.* **95**, 23 (2015).
52. N. Chandra and P. Dang: Atomistic simulation of grain boundary sliding and migration. *J. Mater. Sci.* **34**, 655 (1999).
53. B.W. Huang, J.X. Shang, Z.H. Liu, and Y. Chen: Atomic simulation of bcc niobium $\sum 5\langle 001\rangle\{310\}$ grain boundary under shear deformation. *Acta Mater.* **77**, 258 (2014).
54. K. Cheng, K. Tieu, C. Lu, X. Zheng, and H. Zhu: Molecular dynamics simulation of the grain boundary sliding behaviour for Al $\sum 5(210)$. *Comp. Mater. Sci.* **81**, 52 (2014).
55. Y. Wang, T. Jiao, and E. Ma: Dynamic processes for nanostructure development in Cu after severe cryogenic rolling deformation. *Mater. Trans.* **44**, 1926 (2003).
56. M. Aramfard and C. Deng: Disclination mediated dynamic recrystallization in metals at low temperature. *Sci. Rep.* **5**, 14215 (2015).
57. K.A. Darling, M.A. Tschopp, A.J. Roberts, J.P. Ligda, and L.J. Kecskes: Enhancing grain refinement in polycrystalline materials using surface mechanical attrition treatment at cryogenic temperatures. *Scr. Mater.* **69**, 461 (2013).

https://doi.org/10.1557/jmr.2016.70 Published online by Cambridge University Press